

Patterned line-illumination mesoscopy with a moving slit for enhancing background suppression in cortex-wide mouse brain imaging

Chaowei Zhuang(庄超玮), Yi Yang(杨懿), and Hao Xie(谢浩)

Citation: Chin. Phys. B, 2026, 35 (**2**): 028704. DOI: 10.1088/1674-1056/adf4a6
http://cpb.iphy.ac.cn; http://iopscience.iop.org/cpb

What follows is a list of articles you may be interested in

Assessing pathological features of breast cancer via the multimodal information of multiphoton and Raman imaging

Bing-Ran Gao(高冰然), Xi-Wen Chen(陈希文), Bao-Ping Zhang(张宝萍), Ivan A. Bratchenko, Jian-Xin Chen(陈建新), Shuang Wang(王爽), and Si-Yuan Xu(许思源)

Chin. Phys. B, 2023, 32 (**11**): 118703. DOI: 10.1088/1674-1056/acea67

Image reconstruction for cone-beam computed tomography using total p-variation plus Kullback–Leibler data divergence

Ai-Long Cai(蔡爱龙), Lei Li(李磊), Lin-Yuan Wang(王林元), Bin Yan(闫镔), Zhi-Zhong Zheng(郑治中), Han-Ming Zhang(张瀚铭), Guo-En Hu(胡国恩)

Chin. Phys. B, 2017, 26 (**7**): 078701. DOI: 10.1088/1674-1056/26/7/078701

Cardiac electrical activity imaging of patients with CRBBB or CLBBB in magnetocardiography

Zhu Jun-Jie (朱俊杰), Jiang Shi-Qin (蒋式勤), Wang Wei-Yuan (王伟远), Zhao Chen (赵晨), Wu Yan-Hua (吴燕华), Luo Ming (罗明), Quan Wei-Wei (权薇薇)

Chin. Phys. B, 2014, 23 (**4**): 048702. DOI: 10.1088/1674-1056/23/4/048702

Modulation of electroencephalograph activities by manual acupuncture stimulation in healthy subjects: An autoregressive spectral analysis

Yi Guo-Sheng (伊国胜), Wang Jiang (王江), Deng Bin (邓斌), Wei Xi-Le (魏熙乐), Han Chun-Xiao (韩春晓)

Chin. Phys. B, 2013, 22 (**2**): 028703. DOI: 10.1088/1674-1056/22/2/028703

Modulation of brain functional connectivity with manual acupuncture in healthy subjects: An electroencephalograph case studying

Yi Guo-Sheng (伊国胜), Wang Jiang (王江), Han Chun-Xiao (韩春晓), Deng Bin (邓斌), Wei Xi-Le (魏熙乐), Li Nuo (李诺)

Chin. Phys. B, 2013, 22 (**2**): 028702. DOI: 10.1088/1674-1056/22/2/028702

Patterned line-illumination mesoscopy with a moving slit for enhancing background suppression in cortex-wide mouse brain imaging

Chaowei Zhuang(庄超玮)[1,†], Yi Yang(杨懿)[1,2,3,4], and Hao Xie(谢浩)[5,6,‡]

[1] *Zhejiang Hehu Technology Co., Ltd., Hangzhou* 311121, *China*
[2] *School of Reliability and Systems Engineering, Beihang University, Beijing* 100191, *China*
[3] *Peng Cheng Laboratory, Shenzhen* 518000, *China*
[4] *Hangzhou Innovation Institute, Beihang University, Hangzhou* 310052, *China*
[5] *Institute of Physics, Chinese Academy of Sciences, Beijing* 100190, *China*
[6] *Yangtze River Delta Physics Research Center Co., Ltd., Liyang* 213300, *China*

(Received 14 May 2025; revised manuscript received 12 July 2025; accepted manuscript online 28 July 2025)

Wide-field mesoscopy provides the capabilities of cortex-wide field of view (FOV), cellular resolution and high frame rate for neuronal imaging in the mouse brain. However, inherent background fluorescence degrades the image quality and hinders neuronal signal extraction. To address this problem, we first introduce a cortex-wide, high-resolution line-illumination mesoscope with a moving slit designed for *in vivo* mouse brain imaging. This system achieves a 6.6×6.6 mm FOV, microscale cellular resolution, a high frame rate of 10 Hz, as well as the background rejection ability. Furthermore, we integrated patterned illumination into the system to enhance the background suppression. Experimental results show that the proposed system successfully captures neurodynamics in the living mouse brain. Compared with conventional wide-field mesoscopes, the cortex-wide patterned line-illumination mesoscope (PLIM) achieves a threefold increase in the signal-to-background ratio (SBR). With patterned illumination integrated, the SBR enhancement further reaches four-and-a-half-fold.

Keywords: wide-field fluorescence imaging, optical sectioning, patterned illumination

PACS: 87.85.Pq, 87.19.lh

DOI: 10.1088/1674-1056/adf4a6 **CSTR:** 32038.14.CPB.adf4a6

1. Introduction

The fluorescence microscope has been an essential tool for structural and dynamic imaging in living mouse brains.[1] Recent research progress in neuroscience reveals that various cognitive processes involve the interaction of distributed brain regions spanning the entire mouse brain.[2–4] Consequently, cortex-wide mesoscopy with cellular resolution and high-speed acquisition[5,6] is required. However, conventional microscopes have an inherent trade-off between the field-of-view (FOV) and spatial resolution due to the space–bandwidth product limitation. With the development of commercial objectives with 0.5 NA and 17 mm FOV[7] and megapixel sCMOS with a large sensor, wide-field epifluorescent microscopy breaks the bottleneck and offers a cortex-wide FOV, diffraction-limited resolution, and high frame rates. Consequently, it has emerged as a promising tool for large-scale cortical imaging. For example, the Firefly microscope[7] and COSMOS macroscope[8] achieve a FOV of more than 6 mm with diffraction-limited resolution at 30 Hz frame rate, while the MFIAS macroscope[9] and RUSH macroscope[10] provide centimeter-scale FOV and micrometric resolution at video rates, enabling cortex-wide imaging in the mouse brain. However, strong background fluorescence generated by wide-field illumination degrades both image contrast and resolution.

To overcome this issue, a variety of background-suppression techniques have been proposed. Structured-illumination microscopy[11] synthesizes several patterned-illumination images to suppress out-of-focus fluorescence. HiLo microscopy[12,13] enhances image quality by combining uniform- and non-uniform-illumination images to extract in-focus information. Deconvolution microscopy applies computational algorithms to remove out-of-focus fluorescence based on the point-spread function (PSF) of the system.[14] Photobleaching imprinting microscopy (PIM)[15] extracts high-order fluorescence signals from photobleaching-induced fluorescence decay to eliminate out-of-focus fluorescence. However, these methods require multi-frame acquisitions to reconstruct a high-contrast image, which inevitably introduces artifacts and lowers the frame rate. Optical-sectioning techniques, including confocal microscopy[16,17] and multiphoton scanning microscopy, physically reject background fluorescence through a detection pinhole or by nonlinear excitation.[18–20]

†Corresponding author. E-mail: zhuangchaowei@hehutek.com
‡Corresponding author. E-mail: xiehao@iphy.ac.cn

© 2026 Chinese Physical Society and IOP Publishing Ltd. All rights, including for text and data mining, AI training, and similar technologies, are reserved.

Due to its point-scanning strategy, laser-scanning confocal microscopy on the Mesolens system requires approximately 200 s to cover a full 6 mm FOV.[21] The two-photon random-access mesoscope (2p-RAM) offers multiple operating modes, for example, 1.9 Hz at 2.4 μm pixel size for a 4.4 mm×4.2 mm FOV, or 4.3 Hz at 12 μm pixel size for a 6.3 mm×5.4 mm FOV.[22] Similarly, the Diesel2p mesoscope achieves 3.85 Hz for a 5 mm×3 mm FOV at 1.2 μm spatial resolution.[23] The trade-off between FOV, spatial resolution and frame rate prevents these systems from realizing cortex-wide, video-rate acquisition with cellular resolution in the mouse brain. Line-scanning confocal microscopy mitigates this trade-off by placing a narrow slit before the detector[24–26] or by using the rolling-shutter mode of the camera,[27] thereby balancing frame rate and sectioning capability. This approach has enabled *in vivo* mouse-brain imaging, but existing implementations lack the FOV scalability required for cortex-wide studies.

In this study, we propose a patterned line-illumination mesoscope (PLIM) that incorporates a scanning slit, designed for high-speed cortex-wide imaging with cellular resolution. First, we combined the line-illumination technique with a moving slit to achieve a 6.6 mm FOV, micron-scale resolution, 10 Hz frame rate and effective background suppression capacity. Based on the sparse distribution of neurons, we further applied a patterned illumination strategy that selectively excites neuronal somata, thereby minimizing the background fluorescence. Finally, experimental validation confirms that our system can capture calcium dynamics in neurons across the entire superficial cortex.

2. Materials and methods

2.1. System configuration

A schematic of our PLIM is shown in Fig. 1(a). The illumination beam is generated by a continuous-wave (CW) laser (MBL-III-473-100 mW, CNI, 473 nm central wavelength), which is expanded to a 6 mm diameter via a beam expander. The collimated beam is then reflected by a galvanometer mirror (GVS011/M, Thorlabs), focused by a cylindrical lens (f = 50 mm), and shaped into a linear illumination pattern on a spatial light modulator (SLM) (TSLM023-A, CAS Microstar, 1024×768 resolution, 26 μm pixel pitch). A lens set assembly (Lens 1: f_1 = 75 mm, Lens 2: f_2 = 200 mm, Lens 3: f_3 = 150 mm) relays the SLM pattern to a 2 × /0.5 NA macro zoom objective (MVPLAPO 2XC, Olympus; 137 mm focal length), resulting in 63.3 μm SLM pixel at the sample plane. The line-shaped illumination is scanned across the cortical surface via galvanometer modulation, while emitted fluorescence is collected by the same objective, transmitted through a dichroic mirror, and focused by a 1 × /0.25 NA tube lens (MVPLAPO 1X, Olympus) onto an sCMOS camera (ORCA-Flash4.0, Hamamatsu; pixel size: 6.5 μm). A dual-band emission filter (wavelength: 520±12.5 nm/630±46.5 nm, #87–241, Edmund) is placed in the emission light path to block the reflected excitation laser. The system achieves a 6.6×6.6 mm^2 FOV with 3.25 μm effective pixel resolution. Background suppression is implemented through a virtual moving slit synchronized with the sCMOS rolling shutter, reducing out-of-focus fluorescence.

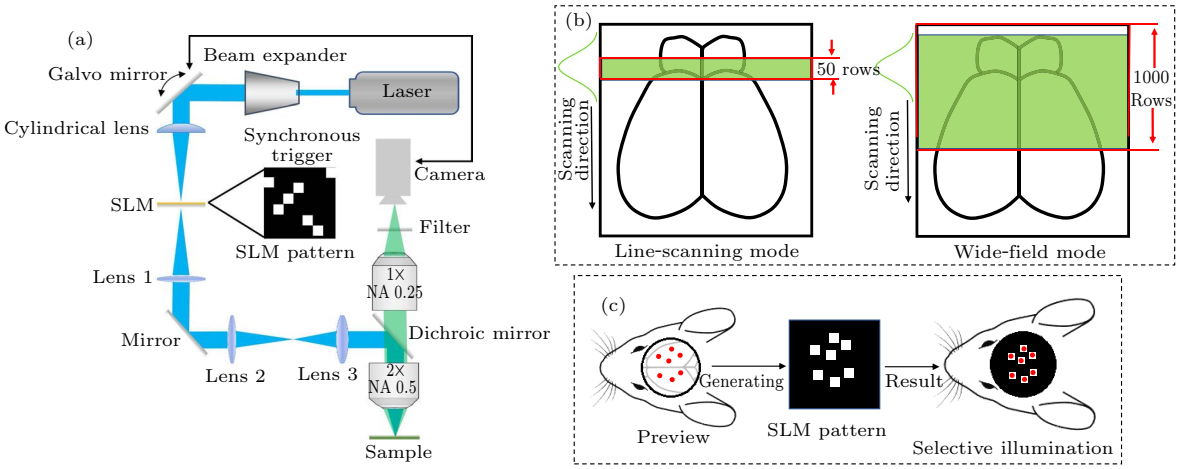


Fig. 1. Principle of the patterned line-illumination imaging. (a) Scheme of the custom-built PLIM, with cortex-wide FOV and cellular resolution. (b) Illustration of line-scanning mode and wide-field mode. (c) Workflow of the patterned illumination.

2.2. Patterned illumination and line-scanning strategy

Our system is able to implement line-scanning mode and wide-field mode with different slit settings, as shown in Fig. 1(b). To eliminate background fluorescence, line-scanning mode was achieved by setting the slit to 50 rows of the sCMOS. To demonstrate better performance of line-scanning mode, we also implemented the wide-field mode by widening the slit to 1000 rows, which minimally rejected background fluorescence, resembling conventional wide-field microscopy. For the optimal imaging, the line-shaped focus scans along the y-axis synchronously with movement of the slit. The synchronization is achieved by a data acquisition

device (NI USB-6353, National Instruments) using a square wave for the sCMOS control and a sawtooth wave for the galvo mirror driver. Figure 1(c) illustrates the principle of patterned illumination. We first acquire 100 frames of the mouse brain and compute a standard-deviation projection. Because neurons exhibit larger fluorescence fluctuations than the background, this projection is used to generate the selective illumination pattern. After threshold-based filtering, the projection is binarized to create the mask. In addition, we pre-calibrate the mapping between the sCMOS camera and the SLM using specific pixels (e.g., the four corner pixels). This calibration allows the designed pattern to be displayed on the SLM so that illumination is restricted to the neuronal regions.

2.3. Animal surgery

Chronic craniotomy was performed according to the procedures described in a previous report in accordance with the guidance of the Animal Care and Use Committees of Tsinghua University. Briefly, a window of 7 mm diameter was created in the mouse brain and a glass coverslip was used to cover the cortex. Then, we mounted a head post to the skull and fixed it with dental cement. During the whole surgical procedure, the mouse was anesthetized using isoflurane (3% in oxygen for induction and 1.5%–2% for surgery and imaging) and a breathing frequency of 1 Hz was maintained. The body temperature was maintained at 37.5 °C with a feedback-controlled blanket, and eye ointment was applied.

3. Results

3.1. System characterization

To evaluate system performance, we first characterized the line-shaped excitation beam at the cortical surface (Fig. 2(a)). The full-width-at-half-maximum (FWHM) of the illumination line was 127 μm, broadened by tissue scattering and background fluorescence. To balance background suppression with signal collection, the virtual slit was set to 50 camera rows, corresponding to 160 μm in the sample plane. The lateral resolution was measured by a 1 μm-diameter green fluorescent microsphere ((T14792, Thermo Fisher Scientific). After Gaussian fitting, we plotted the line profiles along two perpendicular axes and showed the 10 μm lateral resolution in Fig. 2(b), which was sufficient for soma imaging. We further tested the optical sectioning capability quantitatively by axially translating a single green fluorescent microsphere. The fluorescence energy was calculated by averaging the pixel values from the selected region at each depth, as shown in Fig. 2(c). The reference point (Depth = 0 μm) was set as the focal plane of the system. Wide-field detection mode showed $< 5\%$ intensity change with the depth change, but the fluorescence energy changed obviously for the line-scanning mode. The energy decreased below 50% at 60 μm depth, proving the sectioning capability of our line-illumination mesoscope. It is worth noting that, in wide-field mode, the fluorescence signal should ideally remain constant; the observed 5% variation is attributed to residual background fluctuations. In addition, unavoidable contributions from nearby fluorescent microspheres can influence the measurement, even though we attempted to isolate the target bead. These factors likely explain why the peak intensity does not coincide exactly with the reference (focal) plane in wide-field detection. Finally, we measured the pixel size of the SLM and found that it corresponds to 70 μm on the focal plane, as shown in Fig. 2(d), consistent with the theoretical value of 63.3 μm given the system's 3.25 μm sampling resolution.

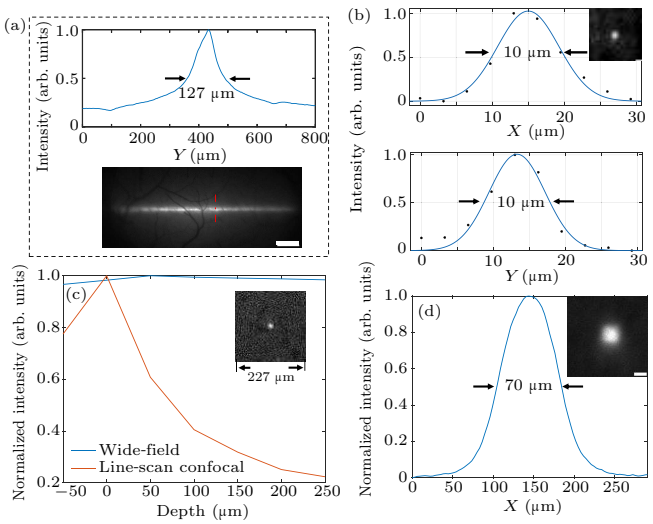


Fig. 2. System characterization of PLIM. (a) Lateral intensity profiles of the line-shaped excitation beam at the brain surface. Scale bar: 500 μm. (b) Experimental PSF. Scale bar: 15 μm. (c) Fluorescence intensity versus axial depths. (d) Lateral intensity profiles of the SLM pixel projection on the focal plane. Scale bar: 60 μm.

3.2. *In vivo* mouse brain imaging by cortical-wide LIM

We then showed that our system enables *in vivo* dynamic neuro-imaging in Ai148 (TIT2L-GC6f-ICL-tTA2)-D; Rasgrf2-2A-dCre (JAX 030328, JAX 022864) mouse brains, which expresses Gcamp6f in cortical layer 2/3. For neuronal imaging in the mouse brain, the illumination power was 100 mW and the frame rate was 10 Hz in both modes. Line-scanning mode was achieved by setting 50 rows of the camera as the slit. Figure 3(a) showed the standard deviation (SD) projection from 750 time-lapse images, covering 6.6 mm FOV with cellular-level resolution. To better show the capability of our system, two subregions were magnified in Fig. 3(b), and the neurons in both subregions were clearly identified. We selected ten neurons in each subregion and plotted the fluorescence signal fluctuation ($\Delta F/F_0$) traces, as shown in Fig. 3(d). F_0 was defined as the average fluorescence intensity out of the soma region, F was defined as the average fluorescence intensity in the marked neuron soma,

and $\Delta F = F - F_0$. To compare our cortical-wide LIM and wide-field mesoscope quantitatively, we calculated $\Delta F/F_0$ values of all spikes of marked neurons. In the line detection mode, the maximum $\Delta F/F_0$ of the spikes was 0.21 and the average $\Delta F/F_0$ was 0.151. Then, we switched our system to wide-field detection mode. Figure 3(c) shows the subregions and selected neurons captured by wide-field detection mode, and Fig. 3(e) plots the $\Delta F/F_0$ curves of the neurons. The maximum $\Delta F/F_0$ of the spikes was 0.066 and the average $\Delta F/F_0$ was 0.044. The results indicate that our system not only achieves cortical-wide FOV and cellular-level resolution, but also enhances the average $\Delta F/F_0$ approximately threefold, compared to the wide-field mesoscope.

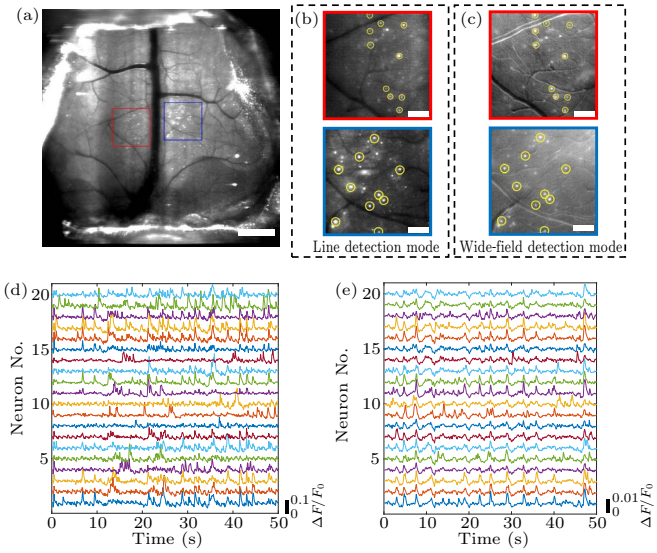


Fig. 3. *In vivo* dynamic neuronal imaging in the mouse brain. (a) Standard deviation projection of 750 time-lapse images in line-scanning mode. Scale bar: 1 mm. (b) Magnified views of the subregions marked in (a). (c) Same subregions captured in wide-field mode. Scale bar: 200 μm. (d), (e) Fluorescence signal fluctuation ($\Delta F/F_0$) of neurons in the yellow circles marked in (b), (c).

3.3. *In vivo* mouse brain imaging by cortex-wide PLIM

To further improve the background suppression, we integrated patterned illumination into our cortex-wide high-resolution LIM. To determine the SLM pattern, we captured 100 time-lapse images in the mouse brain to obtain the location of neurons. The frame rate was set to 10 Hz for both line-scanning mode and wide-field mode. Figure 4(a) shows the SD projection of 1000 time-lapse images of the mouse brain captured by PLIM, with 55 neurons labeled by red circles for fluorescence signal fluctuation ($\Delta F/F_0$) plotting, as shown in Fig. 4(d). The maximum $\Delta F/F_0$ of the spikes was 0.679 and the average $\Delta F/F_0$ was 0.31. To better demonstrate the background suppression capability of PLIM, we compared PLIM, LIM and the patterned illumination wide-field mesoscope (PI-WF) on the same neurons with the same frame rate. Figures 4(e) and 4(f) show the fluorescence signal fluctuation ($\Delta F/F_0$) curves captured by the LIM and PI-WF, respectively. For the LIM, the maximum $\Delta F/F_0$ was 0.384 and the average $\Delta F/F_0$ was 0.212, and for the PI-WF, the maximum and average values were 0.283 and 0.166, respectively. The statistical results are presented in Fig. 4(g). Although integrated with the patterned illumination method, the background suppression capability of the PI-WF remained inferior to that of LIM. The results indicate that the PLIM improved the mean $\Delta F/F_0$ by 50% relative to LIM, achieving a four-and-a-half-fold enhancement over the conventional wide-field mesoscope.

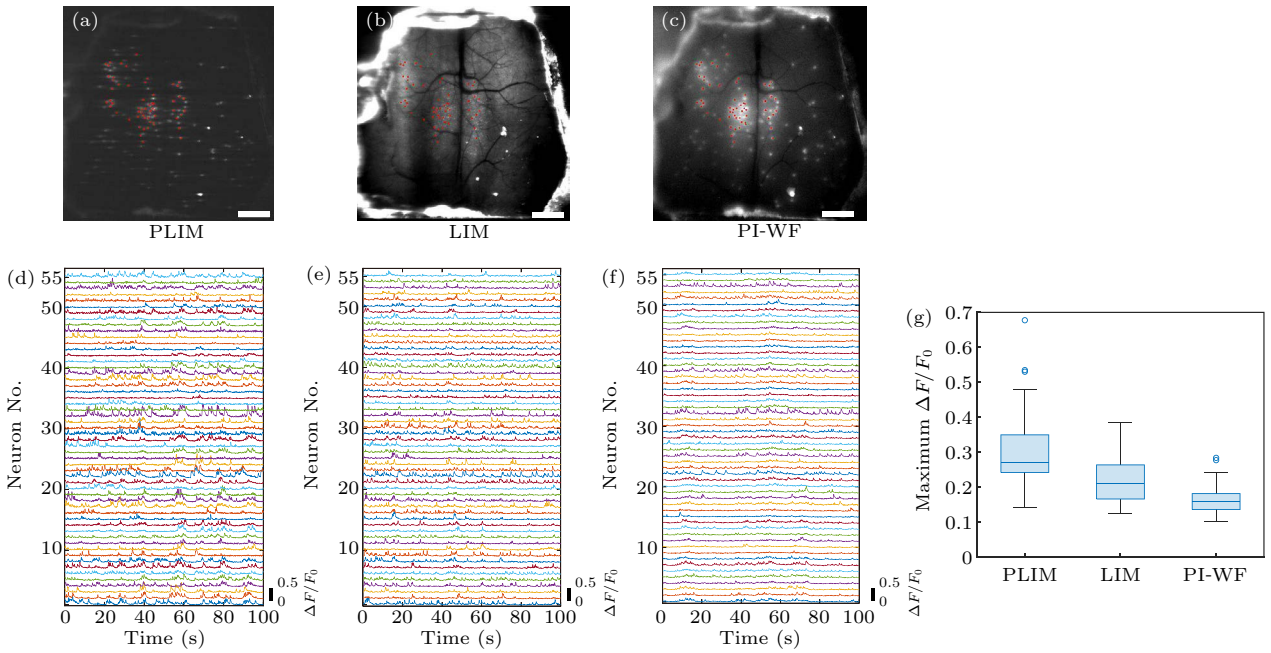


Fig. 4. Comparison of PLIM, LIM and PI-WF in *in vivo* dynamic neuronal imaging. (a)–(c) The standard deviation projections of 150 time-lapse frames by PLIM (a), LIM(b) and PI-WF(c). Scale bar: 1 mm. (d)–(f) Fluorescence signal fluctuation ($\Delta F/F_0$) of neurons marked by red circles in (a)–(c). (g) Statistical results of the maximum $\Delta F/F_0$ captured by PLIM, LIM and PI-WF. PLIM: 0.31±0.11; LIM: 0.21±0.06; PI-WF: 0.17±0.04; mean±SEM, $n = 55$ neurons.

4. Discussion and conclusion

To optimize the slit width of the system, we evaluated 25, 50, 100, 250 and 500 rows on the camera sensor and quantified the fluorescence intensity. We measured the in-focus and out-of-focus fluorescence in the mouse brain. The in-focus fluorescence (S) was defined as the peak intensity of the neuron soma, and the out-of-focus fluorescence (B) was defined as the intensity around the soma region. Figure 5 shows that both in-focus and out-of-focus fluorescence increased with the slit width. However, we set the slit width to 25 rows from 50 rows, and the out-of-focus fluorescence decreased less than the decrement of the in-focus fluorescence, resulting in the SBR degradation. Consequently, we adopted 50 rows as the optimal slit width for our system.

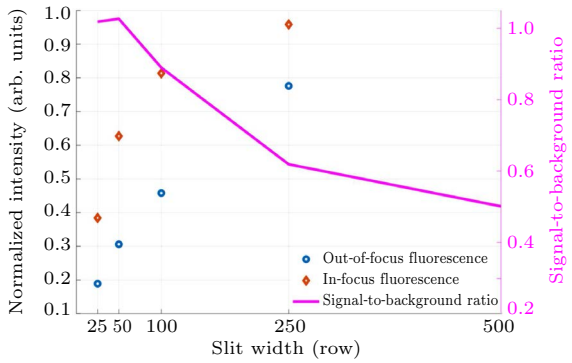


Fig. 5. In-focus and out-of-focus fluorescence with different slit widths.

We also assessed the fluorescence decay attributable to photobleaching and photodamage, observing $< 5\%$ signal loss during 100s of wide-field imaging runs. We also assessed the fluorescence decay attributable to photobleaching and photodamage, observing $< 5\%$ signal loss during 100 s of wide-field imaging runs. Even when this decay is considered, the sequence PI–WF, LIM, PLIM used in Subsection 3.3 introduces only minor variations in $\Delta F/F_0$ that do not alter our conclusions, ensuring a fair comparison between line-scanning and wide-field modes. Importantly, identical laser power was employed for both modalities. Because patterned illumination delivers a higher signal-to-background ratio (SBR), the incident laser intensity can be reduced, thereby further mitigating photobleaching and photodamage.

Compared with wide-field methods, such as COSMOS and RUSH, PLIM offers superior optical sectioning and signal-to-noise ratio for *in vivo* calcium imaging in mouse cortex, enabling lower excitation power and thus reduced photobleaching. The trade-off is that simultaneous modulation of both excitation and detection paths increases system complexity. Future work will therefore focus on improving compatibility with custom objectives and camera arrays.

In summary, we have demonstrated our cortex-wide PLIM for functional imaging in the mouse brain. The capability of 6.6 mm FOV with cellular resolution allows the PLIM to observe neurodynamics distributed across the entire mouse brain. The patterned illumination method is utilized to suppress background fluorescence and enhance contrast by fully using the properties of line-scanning confocal microscopy. Experiment results demonstrated that the SBR of the cortex-wide LIM is three times higher than that of the wide-field mesoscope. Further applying the patterned illumination, our cortex-wide PLIM improves the SBR four-and-a-half-fold compared to the wide-field mesoscope, demonstrating its practical efficacy for large-scale neural circuit studies.

Acknowledgements

H. Xie gratefully acknowledges the support from the National Natural Science Foundation of China (Grant No. 61971256). C. Zhuang thanks Guihua Xiao from Tsinghua University for the chronic craniotomy.

References

[1] Lichtman J M and Conchello J A 2005 *Nat. Methods* **2** 910
[2] Steinmetz N A, Zatka-Haas P, Carandini M and Harris K D 2019 *Nature* **576** 266
[3] Kim E J, Juavinett A L, Kyubwa E M and Callaway E M 2015 *Neuron* **88** 1253
[4] Roy D S, Park Y G, Kim M E, Zhang Y, Ogawa S K, DiNapoli N, Gu X, Cho J H, Choi H, Kamentsky L, Martin J, Mosto O, Aida T, Chung K and Tonegawa S 2022 *Nat. Commun.* **13** 1
[5] Zhuang C, Cao J, Zhang R, Xiao G, Hu J, Xie H and Dai Q 2021 *Biomed. Opt. Express* **12** 1858
[6] Zhang R, Zhuang C, Wang Z, Xiao G, Chen K, Li H, Tong L, Mi W, Xie H and Cao J 2022 *Biosensors* **12** 567
[7] Werley C A, Chien M P and Cohen A E 2017 *Biomed. Opt. Express* **8** 5794
[8] Kauvar I V, Machado T A, Yuen E, Kochalka J, Choi M, Allen W E, Wetzstein G and Deisseroth K 2020 *Neuron* **107** 351
[9] Xie H, Han X, Xiao G, Xu H, Zhang Y, Zhang G, Li Q, He J, Zhu D, Yu X and Dai Q 2023 *Nat. Biomed. Eng.* **8** 740
[10] Fan J, Suo J, Wu J, Xie H, Shen Y, Chen F, Wang G, Cao L, Jin G, He Q, Li T, Luan G, Kong L, Zheng Z and Dai Q 2019 *Nat. Photonics* **13** 809
[11] Neil M, Juskaitis R and Wilson T 1997 *Opt. Lett.* **22** 1905
[12] Lim D, Ford T N, Chu K K and Mertz J 2011 *J. Biomed. Opt.* **16** 016014
[13] Shi R, Jin C, Xie H, Zhang Y, Li X, Dai Q and Kong L 2019 *Biomed. Opt. Express* **10** 6625
[14] McNally J G, Karpova T, Cooper J and Conchello J A 1999 *Methods* **19** 373
[15] Li C, Gao L, Liu Y and Wang L V 2013 *Appl. Phys. Lett.* **103** 183703
[16] Zhao W, Feng Z and Qiu L 2007 *Chin. Phys.* **16** 1624
[17] White J G, Amos W B and Fordham M 1987 *J. Cell Biol.* **105** 41
[18] Denk W, Strickler J H and Webb W W 1990 *Science* **248** 73
[19] Helmchen F and Denk W 2005 *Nat. Methods* **2** 932
[20] Zhang N, Zhou L, Liu X, Wei Z, Liu H, Lan S, Meng Z and Fan H 2021 *Chin. Phys. B* **30** 044204
[21] McConnell G, Tragardh J, Amor R, Dempster J, Reid E and Amos W B 2016 *Elife* **5** e18659
[22] Sofroniew N J, Flickinger D, King J and Svoboda K 2016 *Elife* **5** e14472
[23] Yu C H, Stirman J N, Yu Y, Hira R and Smith S L 2021 *Nat. Commun.* **12** 6639
[24] Wolleschensky R, Zimmermann B and Kempe M 2006 *J. Biomed. Opt.* **11** 064011
[25] Poher V, Kennedy G T, Manning H B, Owen D M, Zhang, H X, Gu E, Dawson M D, French P MW and Neil M AA 2008 *Opt. Lett.* **33** 1813
[26] Jeong H W, Kim H J, Eun J, Heo S, Lim M, Cho Y H and Kim B M 2015 *Appl. Opt.* **54** 3811
[27] Mei E, Fomitchov P A, Graves R and Campion M 2012 *Journal of Microscopy* **247** 269